ELSEVIER

Journal of Molecular Catalysis A: Chemical 115 (1997) 405–419

JOURNAL OF MOLECULAR CATALYSIS A: CHEMICAL

The cluster approach to molecular heterogeneous catalysis [1]

R.A. van Santen

Schuit Institute of Catalysis, Laboratory of Inorganic Chemistry and Catalysis, Eindhoven University of Technology, P.O. Box 513, 5600 MB Eindhoven, The Netherlands

Abstract

Density functional theory enables quantitative computational analysis of reaction intermediates. The cluster approach makes application to heterogeneous catalysis possible. Two cases, one from transition metal catalysis, the other from zeolite catalysis will be analyzed. It will be shown that the information obtained on the elementary reaction steps from cluster calculations can be used to predict the overall rate of a catalytic reaction. In transition metal catalysis CH activation and CO oxidation will be discussed. In zeolite catalysis methanol activation and the hydroisomerization of hexane are treated.

1. Introduction

Heterogeneous catalytic reactions occur on solid surfaces. Hence it may seem that heterogeneous catalytic site models based on clusters cannot properly describe the surface chemistry that is the basis to heterogeneous catalysis. Clearly those aspects of the reaction that intrinsically relate to the presence of the extended lattice or micropore cannot be described by cluster models but require full consideration of the two-dimensional or three-dimensional geometry. Surface reconstruction and island formation belong to this category. In zeolites the shape and size of the micropore cavities may prevent particular reaction paths when transition states are too bulky.

Hence it is important to discriminate between those aspects of the reaction that depend on local properties, that often can be treated using a cluster approach and those aspects of the reaction that are not.

Here we will discuss this for examples from transition metal catalysis and solid acid catalysis by zeolites. In both cases we will use clusters to analyze the transition states of elementary reaction steps and we will demonstrate how this information can be used to predict the overall rate of a catalytic reaction. For the case of catalysis by a transition metal we will apply kinetic Monte Carlo methods to analyze the occurrence of oscillations in the rate of CO oxidation.

In zeolite catalysis we will simulate the turn over frequency (TOF) of hexane isomerization in mordenite and ZSM-5. Here it appears essential to include the structure of the lattice that determines the difference in the heats of adsorption of the reacting molecules.

Clusters are useful in those cases where the surface-chemical bond is localized and where boundary effects are well understood.

[1] Communication presented at the First Francqui Colloquium, Brussels, 19–20 February 1996.

PII S1381-1169(96)00347-0

Quantum-chemical research on clusters has become fruitful especially due to advances in the development of density functional theory techniques and the incorporation of gradient correction terms to the exchange-correlation energy. Several computer programs now have efficient procedures to find the geometries that correspond to stationary points on the potential energy surface. Within the harmonic approximation the vibrational normal modes can be found, so that ground and transition state energies as well as entropies can be computed.

This enables the application of Eyring's transition state reaction theory to predict reaction rate constants [1].

We will start with an analysis of cluster size dependence and relaxation effects on Pd clusters [2]. A comparison will be made with slab calculations using the Car–Parinello method [3].

After the discussion of transition metal catalysis, we will analyze methanol activation using protonic clusters. We will show how different reaction paths for dimethylether formation can be analyzed.

Theory here appears to be essential for a proper understanding of carbenium and carbonium ion intermediates [4].

The theoretical concepts will be used in the following analysis of hexane hydroisomerization.

2. Transition metal catalysis

In Section 2.1 we will discuss cluster geometry relaxation of Pd clusters. Section 2.2 will deal with the activation of methane on Co and Ni clusters.

The final section illustrates the use of statistical methods to predict the rate of an overall catalytic reaction. The case discussed will be CO oxidation.

2.1. Site relaxation

Fig. 1 [2,5] shows for a Pd_6 cluster the changes in geometry when an H atom or O

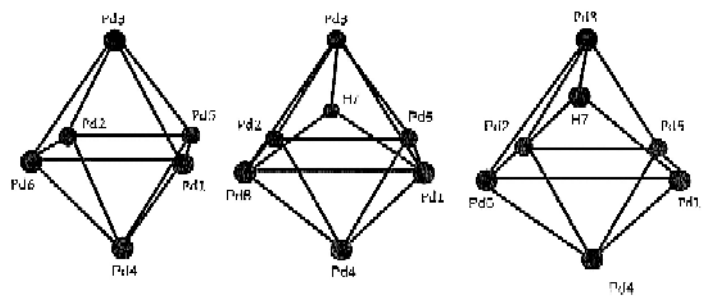

Pd6 Triplet		Pd6 Singlet			Pd6H Doub		Pd6O Trip	
1-3	2.758	1-3	2.697		1-3	2.918	1-3	3.131
1-6	2.631	1-6	2.698		1-6	2.898	1-6	3.074
3-6	2.758	3-6	2.697		3-6	2.918	3-6	2.918
2-4	2.756	2-4	2.697		2-4	2.687	2-4	2.651
2-6	2.632	2-6	2.697		2-6	2.756	2-6	2.757
4-5	2.757	4-5	2.697		4-5	2.681	4-5	2.628
					1-7	1.768	1-7	2.068
				Pd–X	3-7	1.768	3-7	2.068
					6-7	1.767	6-7	2.068

Primary effects (local)

Fig. 1. (a) Pd_6, Pd_6H, Pd_6O cluster geometries. (b) $Pd_{18}H$ cluster geometry. (c) $Pd_{18}O$ cluster geometry [2].

(b)

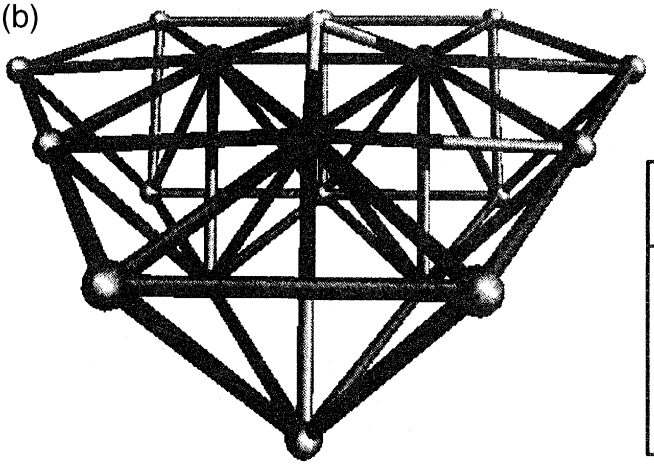

	Pd18 fixed	Pd18 Opt
Pd–H	1.78	1.75
Pd –Pd		
local–local	2.75	2.82
local–next neighbor	2.75	2.72

- *Three local Pd surface atoms optimized with H.*
- *Structural reconstruction shifts these atoms 0.15 ang. above the surface.*

Pd_{18} O/Pd_{18}

(c)

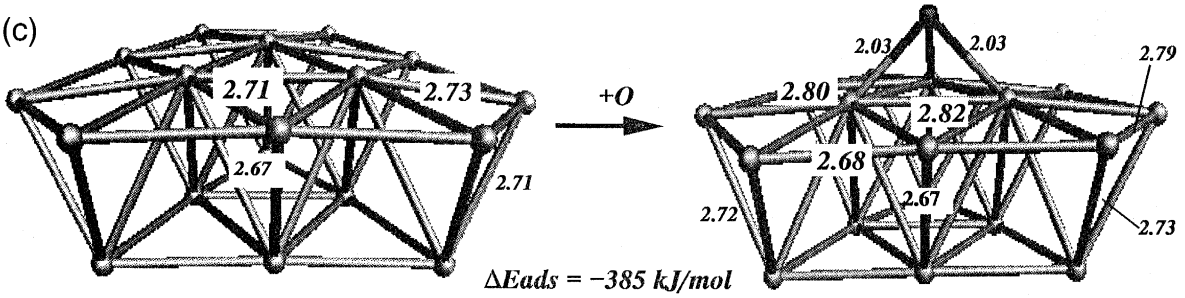

$\Delta Eads = -385$ kJ/mol

($\Delta E_{EXP} = -365$ kJ/mol)

	Pd_{18}	$Pd_{18}O$	
Pd*–Pd *	2.71	2.82	Pd(ads) pulled up by ~0.09 Ang. from surface
Pd–Pd* (neighbor)	2.73	2.80	Pd–Pd Elongated by 0.1 Ang.
Pd–Pd (next nearest)	2.70	2.69	

Fig. 1 (continued).

atom becomes adsorbed to it. The calculated results presented here and in the next paragraphs have been obtained using density functional theory including gradient correction terms.

The magnetic Pd_6 clusters become largely deformed by the coadsorbed atoms. The bonds next to the adsorbed atom change from 0.15 to 0.25 Å.

Large bond distance relaxation and adsorption induced reconstruction effects are common for small particles. However the changes tend to become less dramatic when the metal atom becomes more stabilized by coordination with more neighbors. This we have also found for the interaction of ethylene with very small Pd particles [6]. For very large Pd_{18} particles the

lattice expansions by coadsorption of H or O has reduced to only 0.07 Å (Fig. 1b), with excellent agreement of the computed adatoms bond energies with that to a Pd(111) surface, indicating that bonding has converged to its surface value. The increases in bond distances next to the adatoms are caused by the decrease of the Pd–Pd bond orders due to the involvement of Pd with the additional adsorbing atom. At low surface coverage this leads to a large effective volume of the adsorption site compared to the free site inducing local lattice strain. STM data on C adsorbed to the Ni (100) surface at low surface coverage append to agree with this observation [7]. However at high coverage the expansion in metal–metal bond distance

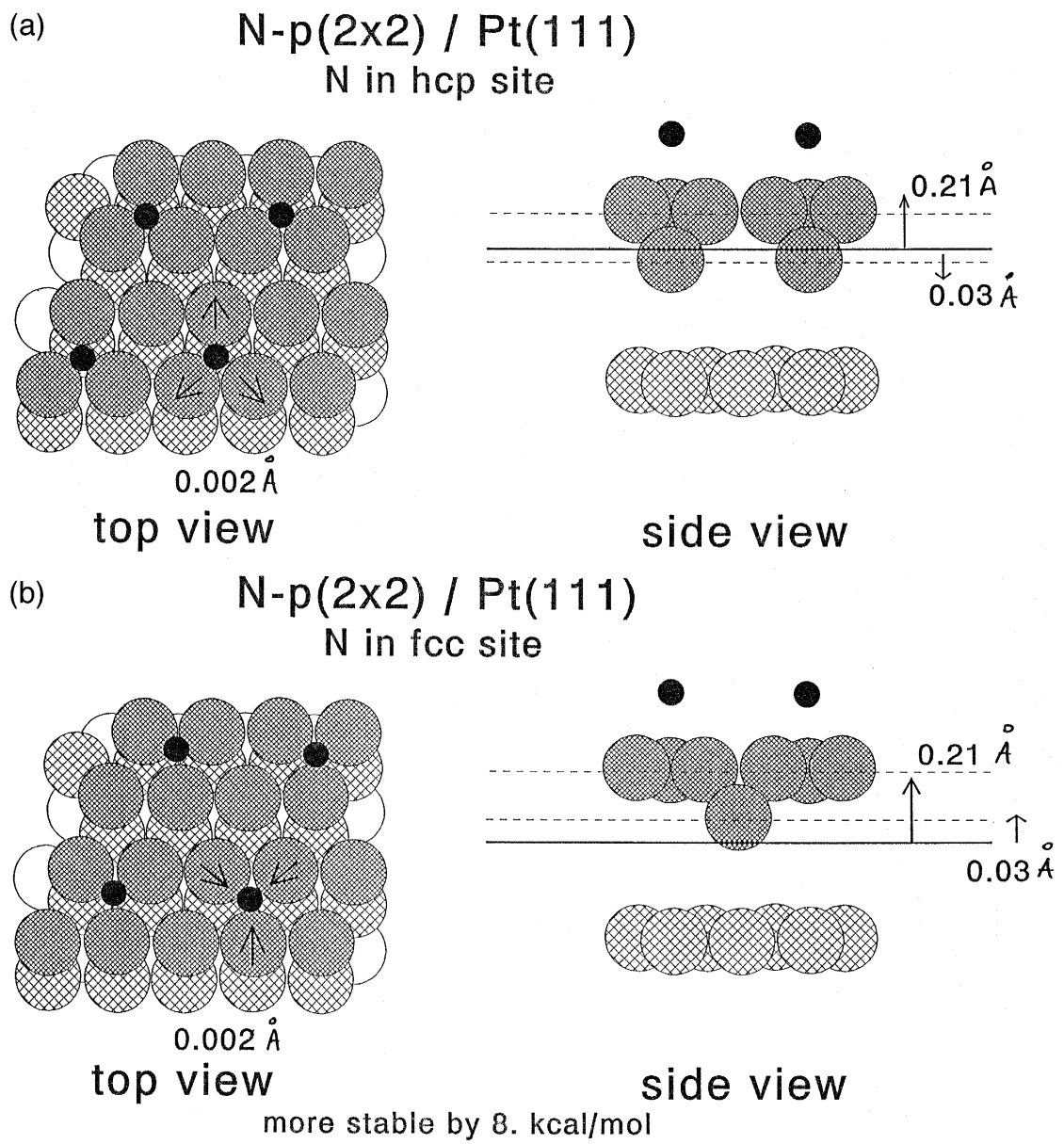

Fig. 2. Car–Parinello predictions of the geometries of N overlayers adsorbed to the two different 3 coordinated positions of the (111) surfaces of Pt [10].

next to the adsorbate has not been experimentally observed. Large surface reconstruction effects are usually reported [8] with displacement of surface atom positions. These changes must be the consequence of the local strain effects that tend to interfere at high surface coverage. Using the Car–Parinello method we have analyzed the relaxation effect on a 3 layer Pt slab with 25% coverage of N [9]. As shown in Fig. 2 very small changes are found in the surface layer, but a large expansion of the bond distances perpendicular to the surface. The expansion of the Pt–Pt bonds in the surface is now prevented because the displacements around different N atoms counteract. The bond weakening effect now only has consequences between the Pt-layers resulting in lattice expansions in close agreement with experiment [9].

One concludes that clusters that simulate surfaces can be used best with fixed bond distances and should be chosen such that boundary effects are minimized.

2.2. The activation energy and rate constant

From a comparison [11] of chemisorption to many different clusters we have concluded that spherical cubo-octahedral clusters of thirteen atoms reproduce the reactivity of (111) surfaces reasonably well. The main advantage of these cluster is the absence of boundary effects, since all exposed atoms are boundary atoms. In Fig. 3

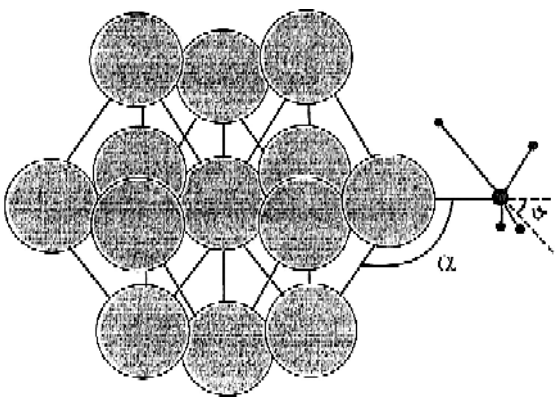

Fig. 3. Transition state of CH_4 dissociation on a Ni_{13} cluster [12].

Table 1
Arrhenius rate parameters for computed rate of CH activation on M_{13} clusters [12]

	Associative desorption	
	pre-exponent ($m^2\ g^{-1}$)	E_{act} (kJ/mol)
Co	2.53×10^{-5}	95
Ni	2.70×10^{-5}	86
	Dissociative desorption	
	pre-exponent ($m^2\ g^{-1}$)	E_{act} (kJ/mol)
Co	7.24×10^{-3}	92
Ni	8.53×10^{-3}	104

such a cluster is shown with the predicted transition state of CH_4 to produce adsorbed H and CH_3. Table 1 shows results for Ni as well as Co. Table 1 shows computed pre exponents as well as activation energies for the rate of dissociative adsorption and associative dissociation [12]. The pre exponents to the reaction rate constants have been obtained by applying Eyring's reaction rate theory expressions [1]. They can be computed from the partition functions of ground- and transition state that depend on the computed vibrational frequencies. The pre-exponents contain information on the mobility in the transition state. In case there is no change in entropy between ground and transition state the pre-exponent is equal to $\sim 10^{13}$ s^{-1}. This is typically found for dissociative or associative surface reactions. The computed activation for dissociative adsorption is within 10 kJ/mol compared to experiment [13]. The decrease in activation energy on Co follows from the larger bond energies of H en CH_3 to Co. According to the Polanyi–Brønsted relation, the change in the activation energy is approximately proportional to the change in reaction energy. This is illustrated in Fig. 4.

One of the most important reasons for the close correspondence between computed and experimental activation energies for dissociation is the proper modelling of the ensemble of surface atoms required for adsorption of the fragments after dissociation. Due to the high

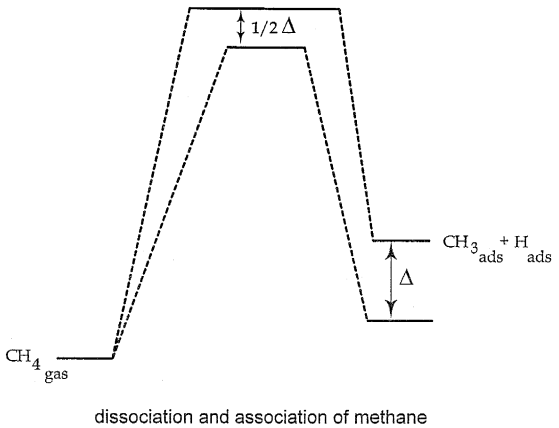

Fig. 4. Brønsted-Polanyi reaction energy plot for dissociative adsorption of CH_4 to Ni and Co.

activation energy the contribution of tunneling to the reaction rate is small. We have estimated this to be of the order of 2 [12]. For a more extensive discussion of transition states of small molecules we refer to [2,14].

2.3. The overall reaction rate of CO oxidation on a Pt(100) surface [15]

Based on the assumption of ideal mixing of adsorbed surface species and concentration independence of the reaction rate constants surface kinetic equations can be formulated and readily solved [1]. Agreement with experiment can be made by fitting rate parameters such that predicted and measured kinetics agree. First principle prediction of these rate parameters

Table 2
Pressures are given in Torr, prefactors in s^{-1}, activation energies in kcal/mol. S_0 stands for initial sticking coefficient [15].

Reaction type	p^{sim}	p^{exp}	S_0^{sim}	S_0^{exp}
CO adsorption	$1\cdot10^{-5}$	$1–3\cdot10^{-5}$	0.8	0.8
O_2 adsorption	$4\cdot10^{-4}$	$2\cdot10^{-4}$	0.1	0.1
	ν^{sim}	ν^{exp}	E_{act}^{sim}	E_{act}^{exp}
CO desorption	$1\cdot10^{15}$	$1–3\cdot10^{15}$	42	28-38
CO_2 production	$2\cdot10^{10}$	10^{10}	20	12–24
1x1 → hexagonal transformation	$1\cdot10^{9}$	—	25	25
Nucleation	0.03	—	0	0
Trapping	0.03	—	0	0

Table 3

Oscillatory regime simulation	experiment
r(CO ads.) < r(O_2 ads.)	r(CO ads.) < r(O_2 ads.)
470 K < T < 510 K	460 K < T < 540 K
period around 200 s	period of 150-200 s

For experimental values, see e.g. Ref. [18].

requires an understanding how these 'intrinsic' parameters, relate to the 'apparent' rate constants and interaction energies of the actual adsorbates on the surface. Statistical methods as Monte Carlo techniques can be used to predict the overall kinetics of a reaction, taking full account of non-ideal surface adsorbate mixing effects that for instance are the consequences of adsorbate island formation. Here we will illustrate the results of the use of a time-dependent Monte-Carlo [16] approach to study the temperature dependence of the oxidation of carbomonoxide catalyzed by the Pt(100) surface in a pressure where rate oscillations are observed [15]. The oscillations are due to a surface phase transformation from the reconstructed low reactivity Pt (100)-hex phase to the reactive non-reconstructed bulk terminated Pt(100) phase [17].

The transformation between the two phases is modelled by a transition between a cubic and hexagonal network that occurs when 5 CO

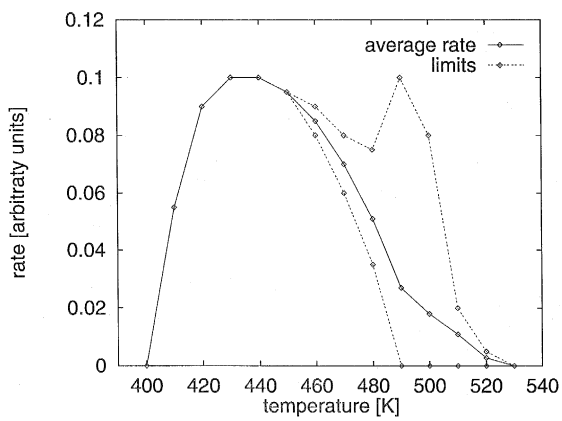

Fig. 5. Temperature dependence of CO oxidation on Pt(100) according to Monte Carlo simulations [15]. The upper and lower limits indicate the maximum and minimum between which the reaction rate oscillates.

molecules become adsorbed next to each other on an ensemble of Pt atoms in the hex configuration. Dissociative adsorption of oxygen only occurs on the non-reconstructed (100) phase. When a surface ensemble of 2 Pt sites is free of adsorbates the (100) transfers back to the (100)-hex configuration.

Tables 2 and 3 gives an overview of the reaction rate parameters used. Pre exponents and activation energies are typical for isolated surface reaction elementary steps. In the table a comparison is made between the predicted and experimental temperature interval [18] where rate oscillations occur and the computed and experimental oscillation frequencies.

Fig. 5 gives the temperature dependence of the surface reaction rate. Initially the reaction is poisoned by adsorbed O_2. When the temperature increases reaction with CO is initiated and steady state reaction rate behavior is observed. At higher temperatures more O_{ads} is reacted, causing transformations to the cubic configuration so that the reaction rate starts to oscillate. At higher temperatures the reaction rate de-

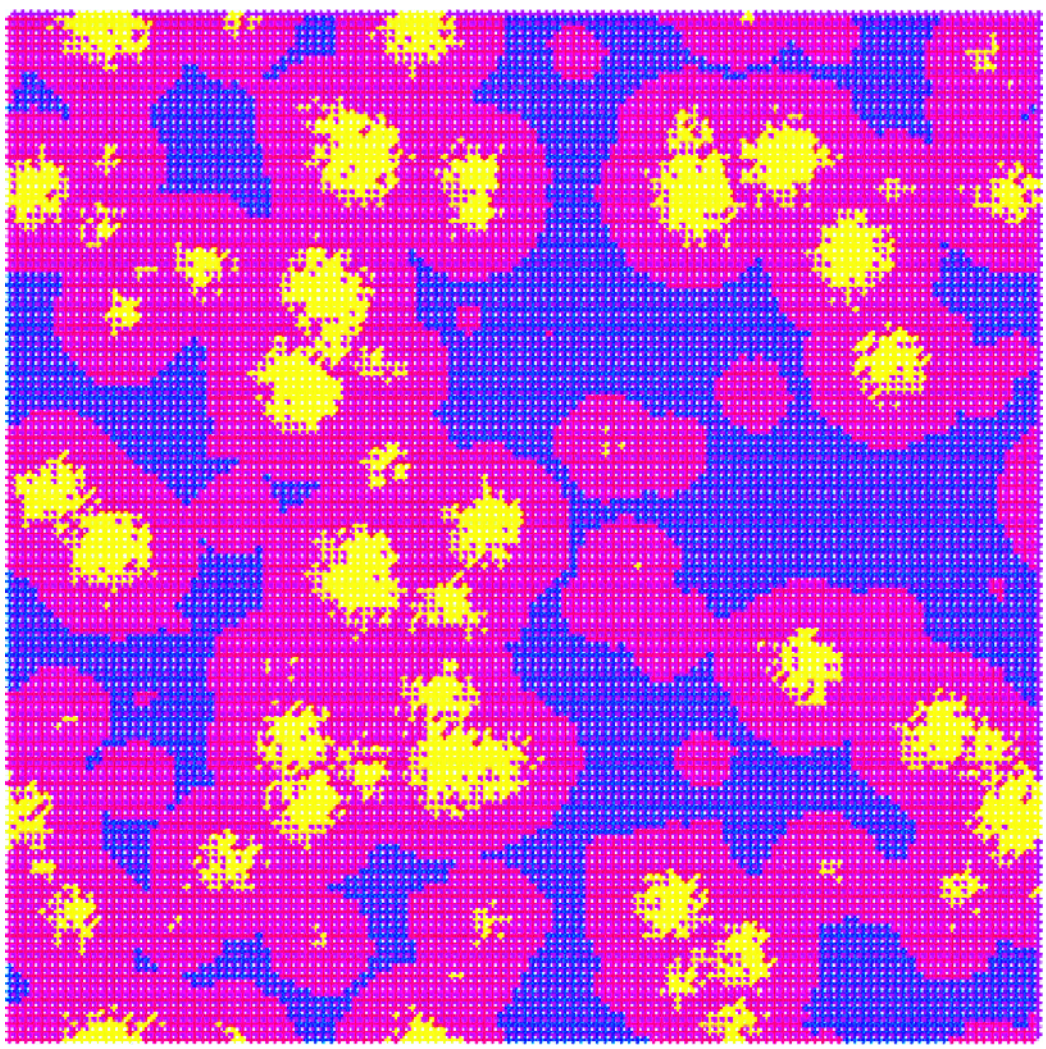

Fig. 6. Island formation through oscillatory regime of CO oxidation [15]. Red areas indicate oxygen adsorbed at the (100) phase, violet areas are CO adsorbed on the (100) phase and yellow areas indicate (100)-hex phase, with low CO coverage.

creases because now CO adsorption becomes rate-limiting.

This approach incorporating phase transformation and incorporating island formation (Fig. 6 shows the presence of islands at oscillatory conditions) can be readily generalized to other systems, with very different energies and rate constants of elementary reaction steps within the islands.

3. Acid catalysis by zeolitic protons

In Section 3.1 quantum-chemical cluster calculations on the activation of methanol to produce dimethylether are presented. Emphasis will be on the mechanism of the reaction. It will be shown that a bimolecular associative mechanism is to be preferred [19]. In Section 3.2 the concepts presented in Section 3.1 will be extended and the modeling of the overall rate of a reaction is studied. The reaction chosen is the hydroisomerization of hexane catalyzed by Pt promoted protonic mordenite and ZSM-5 [20]. The Al/Si rates have been chosen such that the intrinsic acidities of the protons are the same. It will be shown that differences in performance relate to differences in the heats of adsorption of intermediate hexene which are strongly dependent on the zeolite micropore diameter.

3.1. Proton activation of methanol using cluster models

On first sight it appears unlikely that protonation of a molecule by a zeolitic proton can be described well by cutting small cluster from the zeolite. The answer to this question has been extensively investigated [4].

The cluster approximation can be applied to reactions in which the transition state of the reaction or the reaction products are not controlled by the size of the zeolite micro cavities. The usefulness of the cluster approximation deduces from the covalent nature of the chemical bonds in a zeolite. Ninety percent of the bonding can be ascribed to covalent interactions, ten percent to electrostatic interactions.

The proton–oxygen bond in the ground state is highly covalent. Due to the covalent nature of the bonds proton addition to the lattice or protonation of a substrate is accompanied by bond relaxation effects. This bond relaxation can be accommodated by the zeolite lattice by relaxation of the Si–O–Si bond angles. The bending energy of these angles is only of the order of a few kJ/mol varying the angle by 10°. Finally it has been found [21] that three T-atom (three tetrahedra containing) clusters terminated by hydrogen bonds have a deprotonation energy close to that of a very large OH terminated cluster.

Lacking in small clusters is the possibility to study composition dependence or the consequences of hydrogen bonding. For the first, however, successfully larger ring models have been used [22].

The three T-atom clusters terminates by hydrogen atoms can be used to analyze the consequences of acid strength variation by exploiting the covalent nature of the chemical bond [23]. Fig. 7 illustrates this. By changing the bond

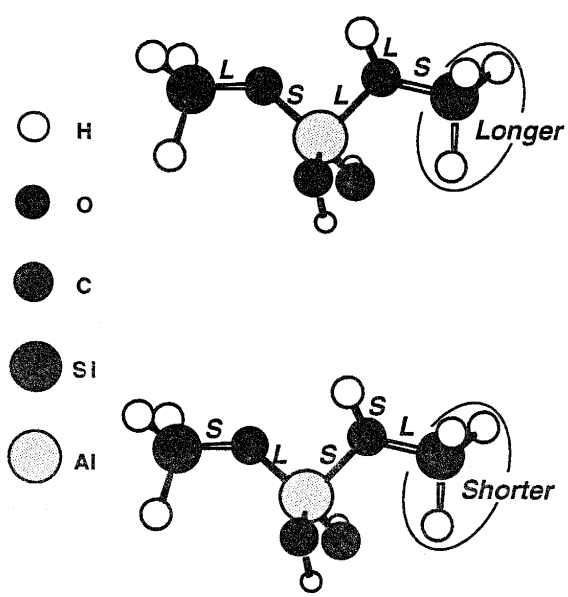

Fig. 7. The zeolitic clusters with shortened or lengthened SiH bonds.

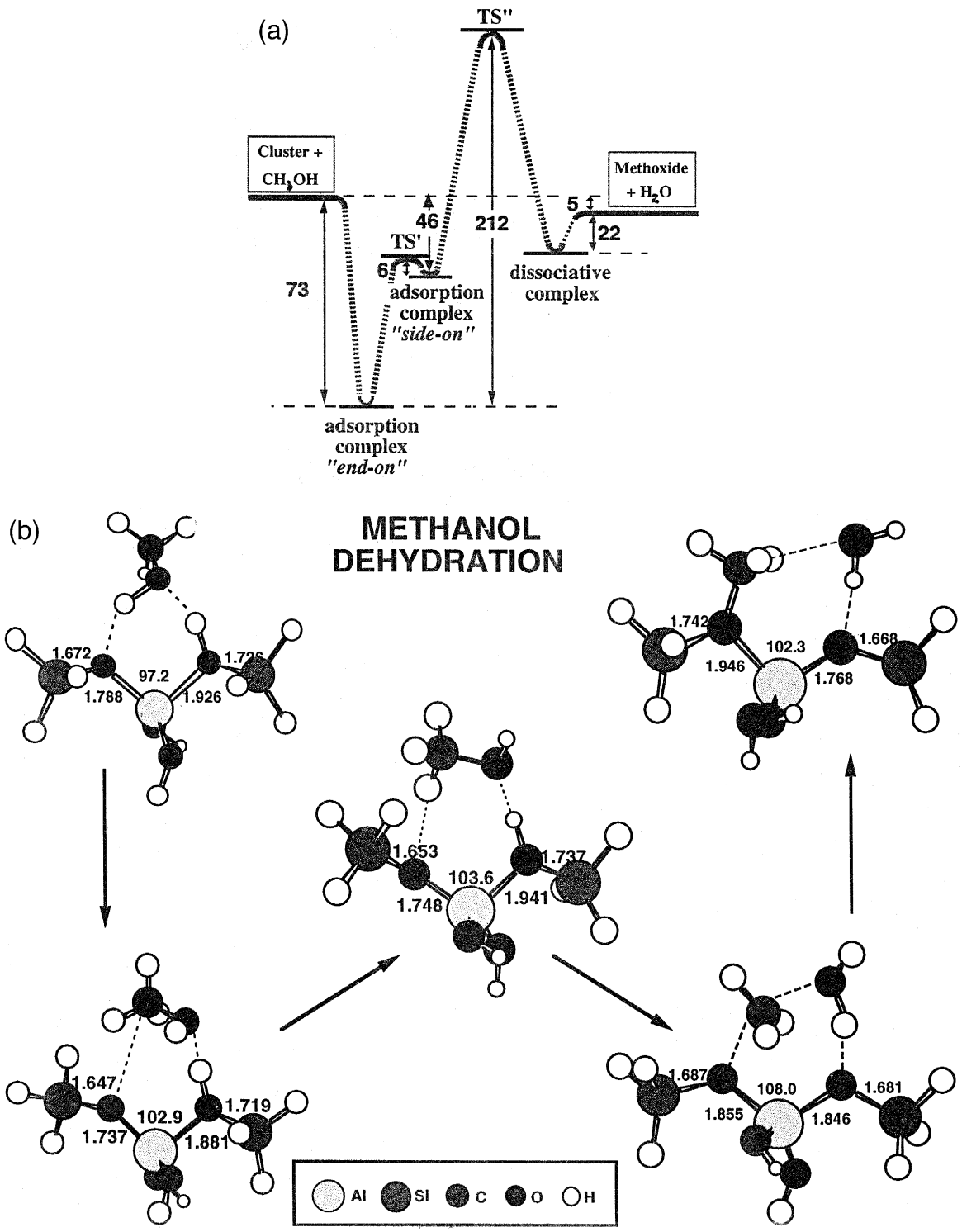

Fig. 8. (a) Computed reaction energy diagram of CH_3OH protolysis. (b) The corresponding structures for ground- and transition states [24].

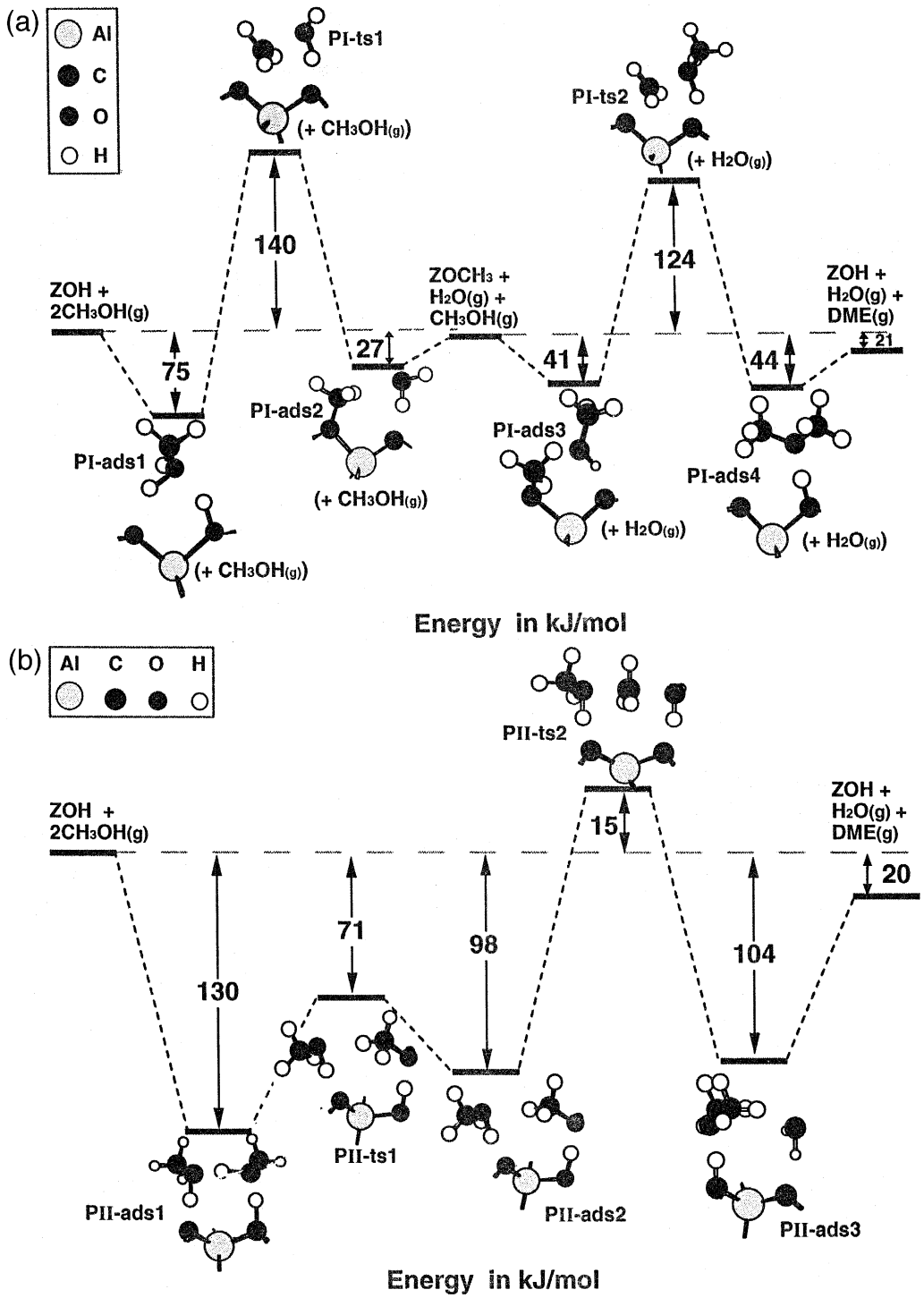

Fig. 9. (a) The reaction energy diagram of dimethylether formation via adsorbed methoxy intermediate. (b) The associative reaction mechanism of dimethylether formation [19].

length of the SiH bonds, the strength of the neighboring SiO bonds is varied and hence the OH bond energy.

Here we will illustrate the use of the cluster approach to analyze proton activation of methanol. It is now well understood [4] that carbenium ions that are intermediates in proton catalyzed reactions cannot freely exist in zeolites. The main reason for this is the absence of stabilizing solvating interactions.

CH_3^+ ions in zeolites however are formed as part of the complex that is the transition state of a proton catalyzed reaction [24]. In the ground state the CH_3^+ ion will be bonded as a methoxy species to the basic oxygen atoms next to Al^{3+} located in the zeolite wall. These covalently bonded methoxy species have been observed by ^{13}C NMR spectroscopy [25].

Fig. 8(a, b) show respectively the energy-reaction diagram and the corresponding intermediate complexes for adsorbed methanol (two different modes), the dissociated product state and the transition states that are formed along the reaction path [24]. One notes the carbenium type structure of the CH_3^+ intermediate in the transition state for C–O cleavage. Proton transfer from lattice to molecule is only observed for the transition state. The high energy with respect to the adsorbed ground state is due to the high energy cost of heterolytic OH splitting. The proton reacts with the OH^- from CH_3OH to form H_2O. The positive charge in the transition state complex resides on the CH_3^+ species and is stabilized by the electrostatic interaction with a basic oxygen atom around Al. This electrostatic stabilization partially compensates for the cost of charge separation when the proton is transferred from the zeolite to methanol.

The overall reaction-energy diagram to dimethylether is shown in Fig. 9a [19]. Dimethylether can be formed by reaction of the adsorbed methoxy species with a second methanol molecule. The overall activation energy with respect to the gas phase is seen to be 140 kJ/mol at low CH_3OH surface coverage and may increase to 215 kJ/mol at high surface coverage. The reaction order will vary between 2 and 0, dependent on the coverage.

The predicted activated energies are not consistent with experiment. Formation of dimethylether is an easy reaction that rapidly proceeds at mild conditions.

We will also analyze an associative reaction route, where reactions occur by direct recombination of methanol molecules. The corresponding reaction energy diagram is shown in Fig. 9b. The ground state is now an associative complex of two methanol molecules. One methanol molecule is bonded to the zeolite lattice via a zeolitic proton. The methanol proton converts to the oxygen atom of the second methanol molecules whose proton is bounded to a basic zeolitic oxygen. The computed infrared spectrum is consistent with experimental data by Mirth et al. [26].

The transition state for methanol formation now corresponds to a Sn_2 nucleophilic substitution reaction. Again we observe the appearance of a carbenium ion intermediate as part of the transition state. Now the overall activation energy varies between 15 kJ/mol for low surface coverage and 145 kJ/mol at high surface coverage, consistent with experimental observations [27]. Hence one concludes that the associative mechanism is the path for dimethylether formation.

We have shown that the methoxy species can react with methanol to methane and formaldehyde by hydride transfer [23]. This process has a high activation energy and therefore may become important at conditions where dimethylether is converted in consecutive reaction steps to ethylene and aromatics.

By varying the Si–H cluster bond length it has been found that hydride transfer is strongly dependent on cluster acidity [23].

The example of dimethylether formation discussed here illustrates the potential of current electronic structure computational methods. It is becoming a predictive tool to study reaction intermediates and transition states. The main current limitation is the small size of the clus-

ters used so that zeolite cavity effects and composition dependence can be only indirectly deduced. The use of Car–Parinello techniques to the study of zeolite reactivity promises a major breakthrough in that extended systems can also be studied with the same accuracy as cluster models. The major issue to be resolved is the accuracy of pseudopotentials applied [28,29].

3.2. Modelling the hydroisomerization of hexane [20]

The hydroisomerization reaction was chosen to analyze kinetics of a zeolite catalyzed reaction. The advantage of this reaction is its stability with time. The primary aim of this study was to demonstrate that the turn-over frequency (TOF) per proton of a zeolite catalyzed reaction may differ significantly, even when the intrinsic acid strength of the zeolitic protons is the same. The experimental work was done with H-mordenite (Si/Al = 10) and H-ZSM-5 (Si/Al = 28) [20]. The proton chemical shifts (41 ppm with respect to TMS) and OH frequencies (~ 3610 cm^{-1}) for these materials were the same. The mechanism of the hydroisomerization reaction is described by the kinetics scheme shown in Fig. 10. Platinum serves to equilibrate hexane and hexene (steps a and e). Conditions during the reaction are such that the partial pressure of hexene is so low that deactivating oligomerization reactions are suppressed. Once hexene is protonated (step b) it isomerizes (step c). After reaction the proton is backdonated and isohexene desorbs (step d), to be hydrogenated over platinum. At high H_2/hexane ratio and large Pt/H^+ ratio equilibration by platinum is fast and the rate-limiting step of the reaction is the rate of isomerization of protonated hexene. Under those conditions one deduces the following expression for the rate of hexane isomerization:

$$\frac{\mathrm{d}[\text{isohexane}]}{\mathrm{d}t} = k_{\text{iso}} \cdot \frac{K^{\text{p}}_{\text{ads}} \cdot K_{\text{eq}} \cdot ([\text{hexane}]/[\text{H}_2])}{1 + K_{\text{ads}} \cdot K_{\text{eq}} \cdot ([\text{hexane}]/[\text{H}_2])} \quad (1a)$$

$$= k_{\text{iso}} \cdot \left\{ K^{\text{p}}_{\text{ads}} \cdot K_{\text{eq}} \cdot \frac{[\text{hexane}]}{[\text{H}_2]} \right\}^{n} \quad 0 < n < 1 \quad (1b)$$

k_{iso} is the rate of isomerization of protonated hexane, $K^{\text{p}}_{\text{ads}}$ is the equilibrium constant of protonation of hexene and K_{eq} is the equilibrium constant of the hexane/hexene equilibrium. Fig. 11 shows the large dependence of the heat of adsorption of alkanes to zeolite structure. Hence $K^{\text{p}}_{\text{ads}}$ may be expected to be strongly zeolite structure dependent. The heat of adsorption and alkanes and alkenes do not differ more than 1 kJ/mol. One finds a correlation of the heat of adsorption with the micropore diameter. For zeolite micropore diameter in excess of 5 Å, it decreases with micropore diameter for mordenite and ZSM-5; the measured values are

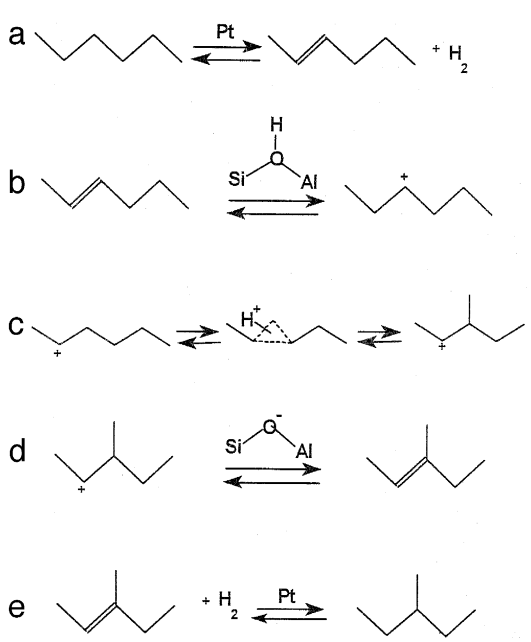

Fig. 10. The bi-functional hydroisomerization reaction mechanism [20]: (a) hexane/hexene equilibration catalyzed by Pt; (b) hexene protonation; (c) isomerization; (d) deprotonation; (e) *iso*-hexene/*iso*-hexane equilibration.

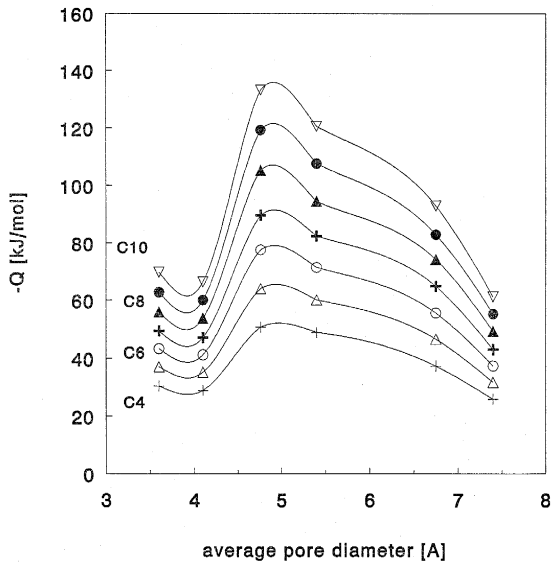

Fig. 11. Computed heats of adsorption of C_nH_{2n+2} hydrocarbons on zeolites with varying pore size dimensions [30].

respectively 72 and 83 kJ/mol. The heat of protonation of hexene can be considered as the sum of two terms (see Fig. 12):

$$\Delta H_{\text{prot. gas}} = \Delta H_{\text{ads}} + \Delta H_{\text{prot. ads}} \quad (2)$$

ΔH_{ads} is the heat of adsorption of hexene with respect to the gas phase and $\Delta H_{\text{prot. ads}}$ is the heat of protonation of adsorbed hexene. ΔH_{ads} is the heat of adsorption of hexene due to the dispersion interaction of hexene with oxygen atoms that form the wall of the zeolite micro cavities.

Table 4
$E_{\text{act,true}} = E_{\text{act, app}} + n\left[\Delta H_{\text{ads}, n=C6} + \Delta H_{\text{prot, ads}} + \Delta H_{\text{dehydr}}\right]$ [20]

Zeolite	$E_{\text{ads}, n=C6}$ (kJ/mol)	$\Delta H_{\text{prot, ads}}$ (kJ/mol)	ΔH_{dehydr} (kJ/mol)	$E_{\text{act, true}}$ (kJ/mol)
MOR	7.19	80	−114.8	125.2
ZSM-5	82	80	−114.8	126.6

The energies of protonation of adsorbed alkenes can be considered independent of the zeolite structure. No measured values are available. However accurate theoretical estimates exist [31] and their values are around 80 kJ/mol. Hence for mordenite and ZSM-5 the protonation energies of hexene with respect to the gas phase become 152 and 163 kJ/mol, respectively. Note that this difference in protonation energy is due to the difference in the heats of adsorption of hexene.

ΔH_{hyd}, the heat of hexane/hexene equilibration can be found from thermodynamics. This enables the determination of $E_{\text{act, iso}}$ from measured reaction orders and apparent activation energy:

$$E_{\text{act, app}} = E_{\text{act, iso}} + n\left(\Delta H_{\text{prot, gas}} + \Delta H_{\text{hydr}}\right) \quad (3)$$

The results are summarized in Table 4.

The predicted values of $E_{\text{act, iso}}$ of 126 kJ/mol is considerably higher than found for isomeriza-

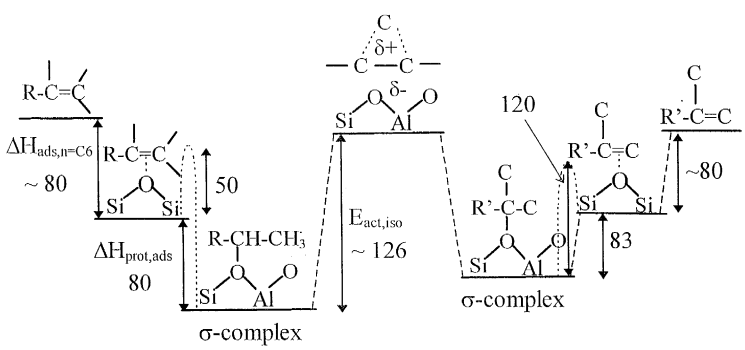

Fig. 12. Reaction energy scheme of isomerization of an olefin by zeolitic proton (kJ/mol). The π-adsorbed state of olefin has not been included [20].

tion reaction in superacidic homogeneous media. There its value is typically 30 kJ/mol [32]. The main reason for the high value of the activation energy for the elementary step of isomerization of the protonated hexene molecule in a zeolite is the strong covalent bond of the alkoxy complex of protonated hexene and the basic zeolite wall oxygen atoms locates around aluminium. The $O_{zeol}-C_{hexyl}$ bond has to be broken so that isomerization can occur in the carbenium type transition state.

We have developed an adsorbate kinetic model [20] based on the concepts so far introduced and find that the differences in measured TOF's expressed per proton due differences in zeolite structure can be completely understood on the basis of the differences in the heats of adsorption of reacting molecules. This can be considered a microscopic basis to Derouane's confinement model [33].

4. Summary

Reaction rate constants of surface chemical reactions can be calculated from first principles using clusters representative of the catalytically active site. Current quantum-chemical calculations enable the prediction of the geometry and energy of ground- and transition states of adsorbed reaction intermediates. Once the corresponding normal-mode frequencies have been computed Eyring's transition state reaction rate theory can be applied to compute the reaction rate constants from the ground state and transition state partition functions. To complete the overall rate of the reaction a kinetic scheme according to the reaction mechanism has to be composed. Statistical techniques like the Monte Carlo method can be used to incorporate non-ideal mixing behavior of the adsorbed surface phase. In case lateral interaction effects can be ignored these equations can be directly integrated to predict reaction orders and apparent activation energies.

References

[1] R.A. van Santen and J.W. Niemantsverdriet, Chemical kinetics and catalysis (Plenum, 1995).
[2] R.A. van Santen and M. Neurock, Catal. Rev. Sci. Eng. 37 (1995) 557.
[3] M. Payne, M.P. Teter, D.C. Allan, T.A. Arias and J.P. Joannopoulos, Rev. Mod. Phys. 64 (1992) 1045.
[4] R.A. van Santen and G.J. Kramer, Chem. Rev. 95(3) (1995) 637.
[5] M. Neurock and D. Dixon, to appear.
[6] A. Fahmi and R.A. van Santen, J. Phys. Chem., to appear.
[7] F. Besenbacher, P.T. Sprunger, L. Ruan, L. Olesen, I. Stensgaard and E. Loegsgaard, Top. Catal. 1 (1994) 325.
[8] F. Besenbacher and J.K. Norskov, Prog. Surf. Sci. 44 (1993) 5.
[9] U. Starke, M.A. van Hove and G.A. Somorjai, Prog. Surf. Sci. 46 (1994) 305.
[10] A. Fahmi, D. Bird and R.A. van Santen, in preparation.
[11] M.C. Zonnevylle, J.J.C. Geerlings and R.A. van Santen, J. Catal. 148 (1994) 417.
[12] H. Burghgraef, A.P.J. Jansen and R.A. van Santen, J. Chem. Phys. 98 (1993) 8810; Surf. Sci. 324 (1995) 345.
[13] P.M. Holmblad, J. Wambach and I. Chorkendorff, J. Chem. Phys. 102 (1995) 8255.
[14] M.A. van Daelen, Y.S. Li, J.M. Newsam and R.A. van Santen, Chem. Phys. Lett. 226 (1994) 100; Y.S. Li, M.A. van Daelen, J.M. Newsam and R.A. van Santen, J. Phys. Chem. 100 (1996) 2279.
[15] R.J. Gelten, A.P.J. Jansen, R.A. van Santen, J.J. Lukkien, J.P.L. Segers and P.A.J. Hilbers, in preparation.
[16] A.P.J. Jansen, Comp. Phys. Comm. 86 (1995) 1; A.P.J. Jansen, Phys. Rev. B 52 (1995) 5400.
[17] G. Ertl, Adv. Catal. 37 (1990) 213.
[18] R. Imbihl, M.P. Cox and G. Ertl, H. Müller and W. Brenig, J. Chem. Phys. 83 (1985) 1578.
[19] S.R. Blaszkowski, R.A. van Santen, J. Am. Chem. Soc., to appear.
[20] A. van de Runstraat, P.J. Stobbelaar, J. van Grondelle, B.G. Anderson, L.J. van IJzendoorn and R.A. van Santen, Proc. Int. Zeolite Conf., Seoul, 1996, Stud. Surf. Sci. Catal.
[21] H.V. Brand, L.A. Curtiss and L.E. Iton, J. Phys. Chem. 96 (1992) 7725.
[22] G.J. Kramer and R.A. van Santen, J. Am. Chem. Soc. 117 (1995) 1766.
[23] S.R. Blaszkowski, M.A.C. Nascimento and R.A. van Santen, J. Phys. Chem. 100 (1996) 3463.
[24] S.R. Blaszkowski and R.A. van Santen, J. Phys. Chem. 99 (1995) 11728.
[25] F.G. Oliver, E.J. Munson and J.F. Haw, J. Am. Chem. Soc. 96 (1992) 8106.
[26] G. Mirth, J.A. Lercher, M.W. Anderson and J. Klinowski, J. Chem. Soc. Faraday Trans. 86 (1990) 3039.
[27] J. Bandiera and C. Naccache, Appl. Catal. 69 (1991) 139.
[28] E. Nusterer, P.E. Blochl and K. Schwarz, Angew. Chem. 108 (1996) 187; B.J. Hammer and J.K. Norskov, Nature 376 (1995) 238; B.J. Hammer, M. Scheffler, K.W. Jacolsen and J.K. Norskov, Phys. Rev. Lett. 73 (1994) 1400; J.A. White,

D.M. Bird, M.C. Payne and I. Stich, Phys. Rev. Lett. 73 (1994) 1404.
[29] R. Shah, M.C. Payne, M.-H. Lee and J.O. Gale, Science 271 (1996) 1395.
[30] S. Bates, W.J.M. van Well, R.A. van Santen and B. Smit, J. Am. Chem. Soc., 28 (1996) 6753.
[31] V.B. Kazansky, M.B. Frash and R.A. van Santen, Appl. Catal., to appear.
[32] D.M. Brouwer and H. Hogeveen, Prog. Phys. Org. Chem. 9 (1972) 179.
[33] E.G. Derouane, J.M. Andre and A.A. Lucas, J. Catal. 110 (1988) 58.